The alignment of smectic A liquid crystals with director tilt on the boundaries

2007 J. Phys. A: Math. Theor. 40 5297

(http://iopscience.iop.org/1751-8121/40/20/005)

IOP PUBLISHING JOURNAL OF PHYSICS A: MATHEMATICAL AND THEORETICAL

J. Phys. A: Math. Theor. **40** (2007) 5297–5318 doi:10.1088/1751-8113/40/20/005

The alignment of smectic A liquid crystals with director tilt on the boundaries

I W Stewart

Department of Mathematics, University of Strathclyde, Livingstone Tower, 26 Richmond Street, Glasgow, G1 1XH, UK

E-mail: i.w.stewart@strath.ac.uk

Received 1 November 2006, in final form 28 February 2007
Published 30 April 2007
Online at stacks.iop.org/JPhysA/40/5297

Abstract

Equilibrium solutions are presented for smectic A liquid crystals in which the usual director **n** and unit layer normal **a** do not necessarily coincide. Previous applications often equate **n** with **a**; the model in this paper allows **n** and **a** to differ and has been motivated by the recent investigations of Auernhammer *et al* (2000 *Rheol. Acta* **39** 215–22, 2002 *Phys. Rev.* E **66** 061707), Soddemann *et al* (2004 *Eur. Phys. J.* E **13** 141–51) and Stewart (2007 *Contin. Mech. Thermodyn.* **18** 343–60). The two experimental geometries studied consist of planar homeotropically aligned smectic layers and 'bookshelf' aligned layers. In both cases a director tilt at the boundaries will be imposed. Solutions to the fully nonlinear bookshelf problem where both the director and the layer normal can vary with an element of decoupling are presented and are particularly relevant to the experimental observations of Elston (1994 *Liq. Cryst.* **16** 151–7); there are two boundary layer effects, as will be discussed, that are related to the biasing of the director towards the smectic A phase and the reorientation of the smectic layers themselves.

PACS numbers: 61.30.−v, 61.30.Dk

1. Introduction

Liquid crystals are anisotropic fluids that generally consist of elongated rod-like molecules which have a preferred local average direction. This direction is commonly described by the unit vector **n**, usually called the director. Smectic liquid crystals are layered structures in which **n** makes an angle θ with respect to the local smectic layer normal **a**, as shown in figure 1. Although the angle θ, also known as the smectic cone angle, is usually temperature dependent, it may, nevertheless, vary because of competition between boundary conditions, elastic effects and smectic layer compressional effects. The idealized smectic A (SmA) liquid crystal phase is said to occur when $\theta \equiv 0$, in which case **n** and **a** coincide as in figure 1(*a*).

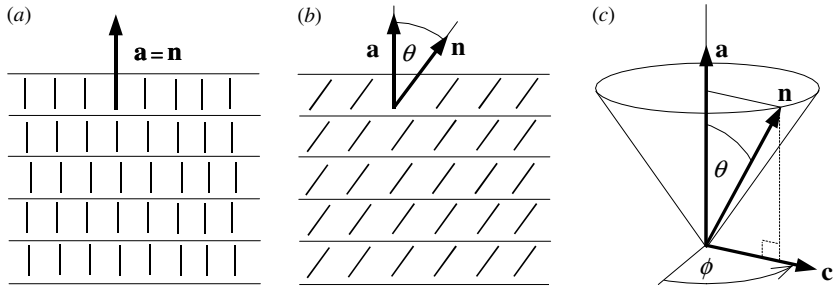

Figure 1. The local layer alignment in smectic liquid crystals. The short bold lines represent the molecular alignment, denoted by the director **n**, within layers. (*a*) The local layer normal **a** coincides with **n** in an idealized SmA. (*b*) **n** may tilt at an angle θ relative to **a**. The idealized SmA phase occurs when $\theta \equiv 0$. (*c*) The director **n** is constrained to lie on the surface of a fictitious cone when $\theta \neq 0$; the vector **c** is the unit orthogonal projection of **n** onto the plane of the smectic layers. In general, the orientation of **n** is completely described by **a** and the angle ϕ that **c** makes measured relative to some axis within the plane of the smectic layers.

When $\theta \neq 0$, the structure is called a smectic C (SmC) liquid crystal. In the SmC phase, the director **n** is constrained to lie on the surface of a fictitious cone, as indicated in figure 1(*c*); it often proves convenient to introduce the unit orthogonal projection of **n** onto the smectic planes, denoted by **c**. In general, the orientation of **n** can be completely described by **a** and **c** because $\mathbf{n} = \cos\theta\mathbf{a} + \sin\theta\mathbf{c}$. The orientation angle ϕ of **c**, measured relative to some fixed axis within the smectic planes, is often introduced in mathematical descriptions of SmC. More general details on the physical and mathematical descriptions of liquid crystals can be found in the books by de Gennes and Prost [6] and Stewart [7].

In this paper, we shall concentrate on liquid crystals that have an inherent desire to be in the SmA phase and assume that the orientation of **c** remains constant relative to some fixed axis within the smectic planes whenever θ is non-zero, so that we can effectively set $\phi \equiv 0$. This assumption is thought to be feasible for many planar-aligned samples of smectic liquid crystal [6, 7] when they are close to the SmA phase; this is known to be the case experimentally [5], especially when flow is absent.

While the director is described by the orientation of **n**, the local planar layer structure may be described by a scalar function Φ, whereby the layer normal is always given by $\mathbf{a} = \nabla\Phi/|\nabla\Phi|$. For example, if uniformly aligned planar smectic layers, such as those depicted in figure 1, lie parallel to the xy plane then $\Phi = z$ leads to $\mathbf{a} = (0, 0, 1)$ in the usual Cartesian description. It is common to assume that **n** and **a** always coincide [6, 7]. However, it has been of interest to model SmA liquid crystals by allowing **n** and **a** to separate [1–4, 8] so that a full description of the director alignment is then provided by **n** and **a** or, equivalently, by **n** and Φ. It is often convenient to employ both **a** and Φ when formulating mathematical descriptions. One of the novel features of this paper is an investigation of equilibrium solutions for the director and smectic layers when **n** no longer necessarily coincides with **a**. We shall impose strong anchoring conditions and suppose that the director and the smectic layers are tilted at the angles θ_0 and δ_0, respectively, on the boundaries. Sometimes, as will be demonstrated in section 2.1, **n** and **a** will coincide precisely over some central region of the sample while they will be able to vary significantly relative to each other near the sample boundaries. However, in general, especially for the problems considered in sections 2.2 and 3, these two vectors will always have at least some small differences between them.

Equilibrium configurations for bounded samples of SmA will be considered, and the equilibrium equations for **n** and **a** will be obtained by minimizing the associated energy integral. A relatively simple energy density, w, will be employed that is based upon the work of Auernhammer *et al* [1, 2, 9], E [10], Ribotta and Durand [8], Soddemann *et al* [3] and Stewart [4]. It has the general form

$$w = \tfrac{1}{2}K_1^n(\nabla\cdot\mathbf{n})^2 + \tfrac{1}{2}K_1^a(\nabla\cdot\mathbf{a})^2 + \tfrac{1}{2}B_0(|\nabla\Phi| + \mathbf{n}\cdot\mathbf{a} - 2)^2 + \tfrac{1}{2}B_1\{1-(\mathbf{n}\cdot\mathbf{a})^2\}, \tag{1.1}$$

with the total bulk energy being given by

$$W = \int_V w\,\mathrm{d}V, \tag{1.2}$$

where V is the sample volume. The energy density w in (1.1) is invariant under the simultaneous changes in sign $\mathbf{n}\to-\mathbf{n}$ and $\mathbf{a}\to-\mathbf{a}$, which is equivalent to invariance under the simultaneous changes $\mathbf{n}\to-\mathbf{n}$ and $\nabla\Phi\to-\nabla\Phi$. The first term on the right-hand side of (1.1) represents the usual elastic splay deformation of the director **n** while the second term is a measure of the bending of the smectic layers; both K_1^n and K_1^a are positive elastic constants. The third term is related to smectic layer compression and is an extended version of that which is known for SmA, based upon the results in [2, 6, 10]; B_0 is the positive layer compression constant. The fourth term is a measure of the strength of the coupling between **n** and **a** with the positive constant B_1 having dimensions of energy per unit volume: in an equilibrium state this energy contribution is clearly minimized when **n** and **a** are parallel. Since **n** and **a** are unit vectors, we note that this term can also be written as $\frac{1}{2}B_1(\mathbf{n}\times\mathbf{a})^2$, as used in [1–3]. Note that the above model does not exclude the possibility that **n** and **a** may coincide at particular locations or regions. We remark further that if $\mathbf{n}\equiv\mathbf{a}$ then the classical nonlinear energy density w_A [10], which makes no distinction between **n** and **a**, can be recovered by setting $K_1 = K_1^n + K_1^a$ to reveal

$$w_A = \tfrac{1}{2}K_1(\nabla\cdot\mathbf{n})^2 + \tfrac{1}{2}B_0(|\nabla\Phi| - 1)^2. \tag{1.3}$$

Nonlinear effects related to the energy in (1.3) have been investigated by Santangelo and Kamien [11]. The energy density stated in (1.1) has recently been applied in a more general dynamic theory by Stewart [4]. The simplified energy density employed by Ribotta and Durand ([8], equation (2)) for SmA under an applied strain, which also drew a distinction between the orientations of **n** and **a**, can be recovered precisely from the nonlinear energy density (1.1) when K_1^a is set to zero, as detailed in appendix A. As remarked in [8], it is expected that the magnitude of B_1 should be comparable to B_0 or smaller. A wide range of values for $B\equiv B_1/B_0$ will be discussed below, and it will be seen that many aspects of the equilibrium solutions are particularly significant when $B<1$.

Equilibrium solutions for the director, corresponding to the minima of W, will be discussed for homeotropically aligned planar samples of SmA in section 2.1. A rigid planar layer approximation to a particular bookshelf alignment of SmA is examined in section 2.2, but it is really section 3 that is directly the most significant for comparisons with experimental observations for bookshelf SmA. In section 3, solutions are found to nonlinear differential equations that describe the variable director and layer structure: the preceding section mostly highlights some key relevant features of the model. A brief discussion of the results is contained in section 4.

2. Fixed smectic layer problems

The first problem to be investigated, in section 2.1, consists of planar homeotropically aligned smectic liquid crystal layers with the layer normal **a** constant throughout. The second

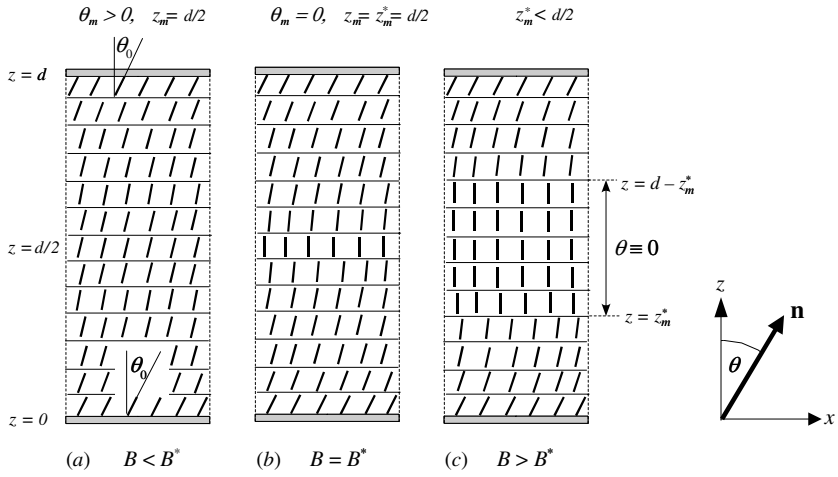

Figure 2. A planar homeotropically aligned smectic sample between boundaries at $z = 0$ and $z = d$. (*a*) The director is strongly anchored at the tilt angle θ_0 at the upper and lower boundaries and θ achieves its minimum value θ_m at $z = z_m = d/2$. (*b*) There exists a value B^* for a given depth d such that $\theta_m = 0$ at $B = B^*$, as detailed in the text after equation (2.30). (*c*) For $B > B^*$ there is a broken extremal with $\theta \equiv 0$ for $z_m^* \leqslant z \leqslant d - z_m^*$ where z_m^* is obtained via the solution of equation (2.23) for any fixed value of $B > B^*$.

problem, in section 2.2, approximates a bookshelf set-up where the director is tilted away from the direction of the layer normal at the boundaries, and the layer structure can again be approximated by assuming a fixed layer normal direction throughout the sample. This second problem gives useful insight to the fully nonlinear bookshelf problem that is of experimental interest in section 3; furthermore, in the solution to the linearized version of the governing equation, a length scale is identified analytically for a boundary layer effect. This will be relevant to the nonlinear variable layer problem that will be explored in section 3.

2.1. Planar homeotropically aligned SmA

We first consider a sample of planar homeotropically aligned smectic liquid crystal confined between boundary plates at $z = 0$ and $z = d$ as pictured in figure 2. The smectic layers are assumed to remain parallel to the boundaries and the director **n** is allowed to tilt within these layers as the layers themselves compress or dilate, with the liquid crystal having an inherent preference to adopt the SmA phase. The director is strongly anchored at the boundaries and makes a fixed angle θ_0, with $0 < \theta_0 < \pi/2$, with respect to the z-axis as shown in figure 2(*a*). This definition of θ_0 coincides with that of the usual SmC average molecular tilt angle (the smectic cone angle) measured relative to the smectic layer normal and is, in this problem, equivalent to a surface pretilt angle of $\psi = \frac{\pi}{2} - \theta_0$, where ψ is the usual measure of director pretilt at the boundary surface. The angle θ_0 is incompatible with the SmA phase in the bulk of the sample. It is therefore expected that the resulting biaxiality induced near the boundaries will weaken towards the centre of the sample as the director attempts to align parallel to the layer normal **a** in the bulk. It will be demonstrated below that this situation is mathematically feasible as elastic effects, layer compression and the coupling between the director and layer structure compete to produce an equilibrium solution for the director profile; moreover, the influence of the coupling constant B_1, which is a novel feature to this work, will become evident. A similar geometry to figure 2 has been investigated by McKay and Leslie [12]

and McKay [13] for planar-aligned SmC liquid crystals; these authors adopted an alternative approach to that developed here and obtained equilibrium solutions for the director via an appropriate SmC energy density.

In the geometry of figure 2, the constant layer alignment is described by $\Phi = z$ with $|\nabla\Phi| = 1$ so that $\mathbf{a} = \nabla\Phi$. The director and the layer normal then take the forms

$$\mathbf{n} = (\sin\theta(z), 0, \cos\theta(z)), \qquad \mathbf{a} = (0, 0, 1), \tag{2.1}$$

where the boundary conditions on $\theta(z)$ are given by

$$\theta(0) = \theta(d) = \theta_0 > 0. \tag{2.2}$$

Only tilt of the director within the xz plane will be considered and it will be supposed, as in [12, 13], that azimuthal twist of the director within the xy plane will be negligible in this simplified model problem. Inserting these forms into the energy density (1.1) gives

$$w = \tfrac{1}{2}K_1^n(\theta')^2\sin^2\theta + \tfrac{1}{2}B_0(1-\cos\theta)^2 + \tfrac{1}{2}B_1\sin^2\theta, \tag{2.3}$$

where a prime denotes $\mathrm{d}/\mathrm{d}z$, and hence the total energy per unit area of the boundary plates is

$$W = \frac{1}{2}\int_0^d \left\{K_1^n(\theta')^2\sin^2\theta + B_0(1-\cos\theta)^2 + B_1\sin^2\theta\right\}\mathrm{d}z. \tag{2.4}$$

A necessary condition for $\theta(z)$ to deliver a minimum value for the energy W is that it satisfies the Euler–Lagrange equation, which is given by

$$\frac{\mathrm{d}}{\mathrm{d}z}\left(\frac{\partial w}{\partial\theta'}\right) - \frac{\partial w}{\partial\theta} = 0. \tag{2.5}$$

In this instance, we are led to the second-order differential equation

$$K_1^n\{\theta''\sin^2\theta + (\theta')^2\sin\theta\cos\theta\} - B_0\sin\theta(1-\cos\theta) - B_1\sin\theta\cos\theta = 0. \tag{2.6}$$

Note that the constant solutions $\theta = 0$ and $\theta = \pm\pi$ are not compatible with the supposed boundary conditions (2.2) and that $\theta \equiv \theta_0$ cannot be an equilibrium solution for any positive values of B_0 and B_1 because $0 < \theta_0 < \pi/2$. This is similar to the situation for the classical case of surface pretilt in nematic liquid crystals when a non-zero magnetic field is applied ([7], pp 82–3). Since w does not contain z explicitly, equation (2.6) has the first integral $w - \theta'\partial w/\partial\theta' = \alpha$, where α is a constant ([14], p 63). Thus the first integral to equation (2.6) can be written as

$$K_1^n(\theta')^2\sin^2\theta = B_0(1-\cos\theta)^2 + B_1\sin^2\theta + C, \tag{2.7}$$

where C is a constant of integration.

Since it is anticipated that the SmA phase is preferred in the bulk, the system will attempt to reduce the director tilt angle from the angle θ_0 imposed at the boundaries. Hence, similar to the conditions often imposed for pretilted nematics [7], a symmetric solution will be sought which fulfils the condition

$$\theta(z) = \theta(d-z) \qquad \text{for} \qquad 0 \leqslant z \leqslant d, \tag{2.8}$$

and satisfies the additional requirement that $\theta(z)$ achieves its minimum, θ_m, at $z = d/2$, that is,

$$\theta'\left(\frac{d}{2}\right) = 0, \qquad \theta\left(\frac{d}{2}\right) = \theta_m \qquad \theta_m \leqslant \theta(z) \leqslant \theta_0. \tag{2.9}$$

The solution will be derived for $0 \leqslant z \leqslant d/2$ with the solution for $d/2 \leqslant z \leqslant d$ being obtained via the symmetry condition (2.8). The constant C in (2.7) can be evaluated using requirement (2.9), which then allows (2.7) to be given as

$$K_1^n\left(\frac{\mathrm{d}\theta}{\mathrm{d}z}\right)^2\sin^2\theta = (B_1 - B_0)(\cos^2\theta_m - \cos^2\theta) + 2B_0(\cos\theta_m - \cos\theta). \tag{2.10}$$

We remark here that the right-hand side of (2.10) can be re-expressed as

$$(\cos\theta_m - \cos\theta)\,[B_1(\cos\theta_m + \cos\theta) + B_0(2 - \cos\theta - \cos\theta_m)]\,, \tag{2.11}$$

which shows that it is strictly positive for all positive values of B_0 and B_1 whenever $\theta_m < \theta(z) \leqslant \theta_0$. Thus we can take square roots of both sides in equation (2.10) to find that

$$\sqrt{K_1^n}\sin\theta\frac{\mathrm{d}\theta}{\mathrm{d}z} = -[(B_1 - B_0)(\cos^2\theta_m - \cos^2\theta) + 2B_0(\cos\theta_m - \cos\theta)]^{\frac{1}{2}}, \tag{2.12}$$

where a minus sign has been chosen in the square root to reflect the expectation that $\theta(z)$ will be decreasing over the interval $0 \leqslant z \leqslant d/2$. Observe also that

$$\left.\frac{\mathrm{d}\theta}{\mathrm{d}z}\right|_{\theta=\theta_m} = \begin{cases} 0 & \text{if} \quad \theta_m > 0, \\ -\sqrt{B_1/K_1^n} & \text{if} \quad \theta_m = 0. \end{cases} \tag{2.13}$$

Note that $\mathrm{d}\theta/\mathrm{d}z$ cannot be evaluated explicitly at $\theta = 0$ via (2.10) if $\theta_m = 0$; a limit, as indicated in (2.13), must be taken.

We now non-dimensionalize by introducing the typical length scale λ, dimensionless parameter B and variable $\bar{z}$ by setting (cf ([6], p 344))

$$\lambda = \sqrt{\frac{K_1^n}{B_0}}, \qquad B = \frac{B_1}{B_0}, \qquad \bar{z} = \frac{z}{\lambda}, \qquad \bar{d} = \frac{d}{\lambda}. \tag{2.14}$$

Equation (2.12) can then be integrated to give the formal solution for $\theta(\bar{z})$ implicitly as

$$\bar{z} = \int_{\theta}^{\theta_0} \frac{\sin\psi}{[(B-1)(\cos^2\theta_m - \cos^2\psi) + 2(\cos\theta_m - \cos\psi)]^{\frac{1}{2}}}\,\mathrm{d}\psi, \qquad 0 \leqslant \bar{z} < \frac{\bar{d}}{2}, \tag{2.15}$$

subject to the formal requirement, arising from (2.9),

$$\frac{\bar{d}}{2} = \int_{\theta_m}^{\theta_0} \frac{\sin\psi}{[(B-1)(\cos^2\theta_m - \cos^2\psi) + 2(\cos\theta_m - \cos\psi)]^{\frac{1}{2}}}\,\mathrm{d}\psi. \tag{2.16}$$

Note also that (2.13) becomes

$$\left.\frac{\mathrm{d}\theta}{\mathrm{d}\bar{z}}\right|_{\theta=\theta_m} = \begin{cases} 0 & \text{if} \quad \theta_m > 0, \\ -\sqrt{B} & \text{if} \quad \theta_m = 0. \end{cases} \tag{2.17}$$

The requirement in (2.16) establishes the value for θ_m for given values of $\bar{d}$, θ_0 and B. This value for θ_m is then inserted into (2.15) to provide the implicit solution for θ as a function of $\bar{z}$. However, equations (2.15) and (2.16) cannot hold for all values of $\bar{d}$ and B, as we shall see below where it will be shown, for any given fixed value of B, that there is a critical value $\bar{z}_m^*$ at which $\theta(\bar{z}_m^*) \equiv \theta_m = 0$ with the property that equation (2.15) is valid for $0 \leqslant \bar{z} \leqslant \bar{z}_m^*$ but is not valid for $\bar{z} > \bar{z}_m^*$, with the consequence that (2.16) cannot be valid for $\bar{d} > 2\bar{z}_m^*$.

Using the substitution $u = \cos\psi$, solution (2.15) becomes

$$\bar{z} = \begin{cases} \dfrac{1}{\sqrt{B-1}}\displaystyle\int_{\cos\theta_0}^{\cos\theta} \left\{\left(\cos\theta_m + \frac{1}{B-1}\right)^2 - \left(u + \frac{1}{B-1}\right)^2\right\}^{-\frac{1}{2}} \mathrm{d}u & \text{if } B > 1, \\ \dfrac{1}{\sqrt{2}}\displaystyle\int_{\cos\theta_0}^{\cos\theta} (\cos\theta_m - u)^{-\frac{1}{2}}\,\mathrm{d}u & \text{if } B = 1, \\ \dfrac{1}{\sqrt{1-B}}\displaystyle\int_{\cos\theta_0}^{\cos\theta} \left\{\left(\frac{1}{1-B} - u\right)^2 - \left(\frac{1}{1-B} - \cos\theta_m\right)^2\right\}^{-\frac{1}{2}} \mathrm{d}u & \text{if } 0 < B < 1. \end{cases} \tag{2.18}$$

The integrals in (2.18) can be evaluated to find ([15, section 2.261])

$$\bar{z} = \begin{cases} \dfrac{1}{\sqrt{B-1}}\{\sin^{-1}(g(\theta,\theta_m)) - \sin^{-1}(g(\theta_0,\theta_m))\} & \text{if} \quad B > 1, \\ \sqrt{2}\{(\cos\theta_m - \cos\theta_0)^{\frac{1}{2}} - (\cos\theta_m - \cos\theta)^{\frac{1}{2}}\} & \text{if} \quad B = 1, \\ \dfrac{1}{\sqrt{1-B}}\{\ln|h(\theta_0,\theta_m)| - \ln|h(\theta,\theta_m)|\} & \text{if} \quad 0 < B < 1, \end{cases} \tag{2.19}$$

where

$$g(\theta,\theta_m) = \frac{1+(B-1)\cos\theta}{1+(B-1)\cos\theta_m}, \tag{2.20}$$

$$h(\theta,\theta_m) = \left\{\left(\frac{1}{1-B} - \cos\theta\right)^2 - \left(\frac{1}{1-B} - \cos\theta_m\right)^2\right\}^{\frac{1}{2}} + \frac{1}{1-B} - \cos\theta. \tag{2.21}$$

Clearly, in all cases, $\bar{z} = 0$ at $\theta = \theta_0$ and $\bar{z}$ increases monotonically from zero as θ decreases from θ_0 to θ_m. Hence θ can achieve a minimum value of $\theta_m > 0$ at $\bar{z} = \bar{z}_m$ where

$$\bar{z}_m = \begin{cases} \dfrac{1}{\sqrt{B-1}}\cos^{-1}(g(\theta_0,\theta_m)) & \text{if} \quad B > 1, \\ \sqrt{2}(\cos\theta_m - \cos\theta_0)^{\frac{1}{2}} & \text{if} \quad B = 1, \\ \dfrac{1}{\sqrt{1-B}}\left\{\ln|h(\theta_0,\theta_m)| - \ln\left|\dfrac{1}{1-B} - \cos\theta_m\right|\right\} & \text{if} \quad 0 < B < 1. \end{cases} \tag{2.22}$$

The maximum possible value for $\bar{z}_m$ occurs at $\bar{z}^*_m$ when $\theta_m = 0$, in which case

$$\bar{z}^*_m = \begin{cases} \dfrac{1}{\sqrt{B-1}}\cos^{-1}(g(\theta_0,0)) & \text{if} \quad B > 1, \\ 2\sin\left(\dfrac{\theta_0}{2}\right) & \text{if} \quad B = 1, \\ \dfrac{1}{\sqrt{1-B}}\left\{\ln|h(\theta_0,0)| - \ln\left|\dfrac{B}{1-B}\right|\right\} & \text{if} \quad 0 < B < 1. \end{cases} \tag{2.23}$$

It follows from (2.23) that $\bar{z}^*_m$ is monotonically decreasing as a function of B and that

$$\bar{z}^*_m \to \infty \quad \text{as } B \to 0^+ \qquad \text{and} \qquad \bar{z}^*_m \to 0 \quad \text{as } B \to \infty. \tag{2.24}$$

Before going on to discuss more details on the dependence of $\bar{z}^*$ upon B, there are two cases to consider.

Case 1. $\bar{d}/2 \leqslant \bar{z}^*_m$. If $\bar{d}/2 < \bar{z}^*_m$ then the full solution for $0 \leqslant \bar{z} \leqslant \bar{d}/2$ is given by (2.19) with $\theta_m > 0$ determined by (2.22) with $\bar{z}_m = \bar{d}/2$. Furthermore, by (2.17),

$$\theta(\bar{z}_m) = \theta_m \qquad \text{and} \qquad \left.\frac{\mathrm{d}\theta}{\mathrm{d}\bar{z}}\right|_{\theta=\theta_m} = 0 \qquad \text{at} \qquad \bar{z} = \bar{z}_m = \frac{\bar{d}}{2} < \bar{z}^*_m. \tag{2.25}$$

If $\bar{d}/2 = \bar{z}^*_m$ then the solution is again provided by (2.19) except that now $\theta_m = 0$ and $\bar{z}_m = \bar{z}^*_m = \bar{d}/2$ with, by (2.17),

$$\theta(\bar{z}^*_m) = 0 \qquad \text{and} \qquad \left.\frac{\mathrm{d}\theta}{\mathrm{d}\bar{z}}\right|_{\theta=0} = -\sqrt{B} \qquad \text{at} \qquad \bar{z} = \bar{z}^*_m = \frac{\bar{d}}{2}. \tag{2.26}$$

This change in the derivative of the solution when θ_m changes from being non-zero to zero signals the possibility of a broken extremal being available whenever $\bar{d}/2 > \bar{z}_m^*$. This leads to consideration of what happens when $\bar{d}/2 > \bar{z}_m^*$.

Case 2. $\bar{d}/2 > \bar{z}_m^*$. For $0 \leqslant \bar{z} \leqslant \bar{z}_m^*$, solution (2.19), in conjunction with (2.23), remains valid. However, despite it being no longer valid for $\bar{z}_m^* < \bar{z} \leqslant \bar{d}/2$, it nevertheless can be extended by setting

$$\theta(\bar{z}) \equiv 0, \qquad \bar{z}_m^* < \bar{z} \leqslant \frac{\bar{d}}{2}. \tag{2.27}$$

This extended solution θ is defined for $0 \leqslant \bar{z} \leqslant \bar{d}/2$ and satisfies the equilibrium equation (2.6) in a 'weak' sense: it is continuous but has a discontinuous derivative at $\bar{z} = \bar{z}_m^*$, as is evident from (2.26) and (2.27). This solution is therefore sectionally smooth with a jump discontinuity in the derivative at $\bar{z} = \bar{z}_m^*$ and so θ, in the notation of Sagan ([14, p 18, section D]), belongs to the space of functions $C^1_{SP}[0, \bar{d}/2]$, where $P = \{\bar{z}_m^*\}$. The solution therefore has a corner at $\bar{z} = \bar{z}_m^*$ and for $\theta \in C^1_{SP}[0, \bar{d}/2]$ to be an equilibrium solution it must additionally satisfy the Weierstrass–Erdmann corner conditions, that is, it must fulfil the left- and right-limit conditions ([14, p 80])

$$\left.\frac{\partial \bar{w}}{\partial \theta'}\right|_{\bar{z}_m^* - 0} = \left.\frac{\partial \bar{w}}{\partial \theta'}\right|_{\bar{z}_m^* + 0}, \tag{2.28}$$

$$\left[\theta' \frac{\partial \bar{w}}{\partial \theta'} - \bar{w}\right]_{\bar{z}_m^* - 0} = \left[\theta' \frac{\partial \bar{w}}{\partial \theta'} - \bar{w}\right]_{\bar{z}_m^* + 0}, \tag{2.29}$$

where a prime now denotes $\mathrm{d}/\mathrm{d}\bar{z}$ and, by (2.3), (2.4) and $(2.14)_3$,

$$\bar{w} = \tfrac{1}{2} B_0 \lambda [(\theta')^2 \sin^2\theta + (1 - \cos\theta)^2 + B \sin^2\theta]. \tag{2.30}$$

It is clear from the results in (2.25) and (2.26) that the corner conditions are satisfied for the extended solution θ.

It now follows that for any $\bar{d}$ and any $B > 0$ we can construct an equilibrium solution to equation (2.6). In the method adopted above, B was fixed and a solution was found that belonged to either $C^1[0, \bar{d}/2]$ or $C^1_{SP}[0, \bar{d}/2]$ (cases 1 and 2 above, respectively), depending on the availability of the point $\bar{z}_m^*$, which obviously depended upon the value of B. The solution type changes at $\bar{z} = \bar{z}_m^*$ and, before giving graphical examples of solutions, it is useful to know the dependency of $\bar{z}_m^*$ upon B. Figure 3 below shows $\bar{z}_m^*$ as a function of B, obtained numerically from the results in equation (2.23). These curves display the qualitative aspects of the dependence of $\bar{z}_m^*$ for the indicated fixed boundary tilt angles. For a fixed depth $\bar{d}$ there will be a critical value $B = B^*$ at which the broken extremal solution becomes available, corresponding to $\bar{z}_m^* = \bar{d}/2$. As an example of the dependence of the minimum value θ_m upon B, figure 4 shows the situation for a director tilt on the boundary set at $\theta_0 = 0.05$ and sample depth $\bar{d} = 0.05$; this graph was obtained from equation (2.22) with $\bar{z}_m^*$ set equal to $\bar{d}/2 = 0.025$ in (2.23) where, in this case, $B^* \doteqdot 3.99$. This behaviour is also evident in the full solutions displayed in figure 5 when $\theta_0 = 0.05$ and $\bar{d} = 0.05$: for these solutions the minimum value of θ for a given value of B equals θ_m for the corresponding value of B in figure 4. These solutions were obtained directly from the implicit solutions presented in equations (2.19) to (2.23) and (2.27). The smooth extremal becomes a broken extremal as B increases. It is also seen from figure 5 that in this particular example broken extremals occur for $B > B^* \doteqdot 3.99$ and that the derivative conditions in (2.25) and (2.26) are evident in accordance with $B < B^*$ or $B > B^*$. Schematic representations of solutions such as those in figure 5 are given in figure 2 (note that $z = \lambda\bar{z}$ and $z_m = \lambda\bar{z}_m$). In correspondence with the results in figure 5, in figure 2(a),

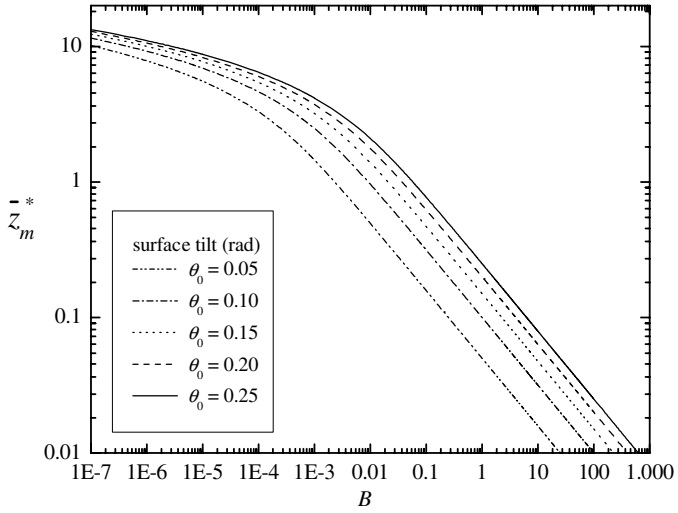

Figure 3. The dependence upon B of the depth $\bar{z}_m^*$ at which a broken extremal first becomes available, obtained from equation (2.23). These are samples of representative plots for the indicated fixed boundary tilt angles θ_0 for the director on the boundary, as defined in figure 2(*a*).

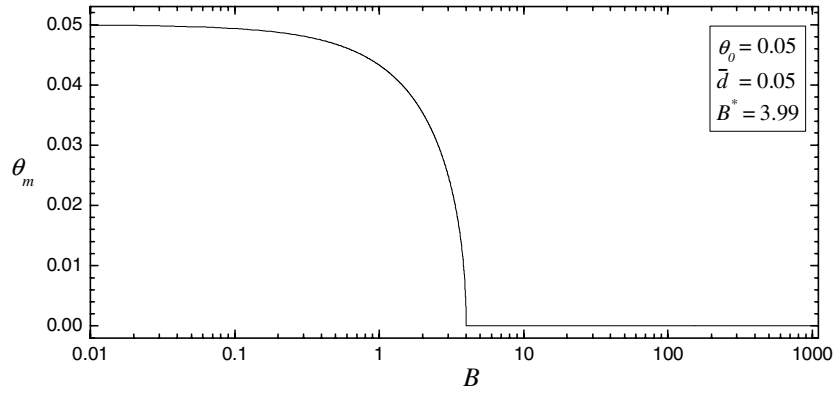

Figure 4. The dependence of the minimum value θ_m upon B for a director tilt on the boundary set at $\theta_0 = 0.05$ radians and sample depth $\bar{d} = 0.05$, obtained from equation (2.22) with $\bar{z}_m^*$ set equal to $\bar{d}/2$ in (2.23).

$B < B^*, 0 < \theta_m < \theta_0$ and there is no broken extremal; in figure 2(*b*), $\theta_m = 0$ at $B = B^*$, which corresponds to the value of B at which $d/2 = z_m^* = \lambda \bar{z}_m^*$, obtained from equation (2.23) or, equivalently, via figure 3; in figure 2(*c*), for any given fixed value $B > B^*$, $\theta(z)$ is a broken extremal with $\theta \equiv 0$ for $z_m^* \leqslant z \leqslant d - z_m^*$ where z_m^* is obtained via equation (2.23).

The solutions shown in the above figures are qualitative for some selected values of director tilt on the boundaries and dimensionless sample depth. For homeotropically aligned planar samples of smectic the penetration depth, which corresponds to z_m^* (note that the calculation of z_m^* is independent of the sample depth d), may be of the order of a small multiple of the smectic interlayer distance d_0. The distance d_0 can be approximated by $d_0 \approx \lambda \approx 20$ Å ([6], p 363). For $z_m^* = \lambda \bar{z}_m^*$ to achieve such values d_0, we would require B to be roughly of an

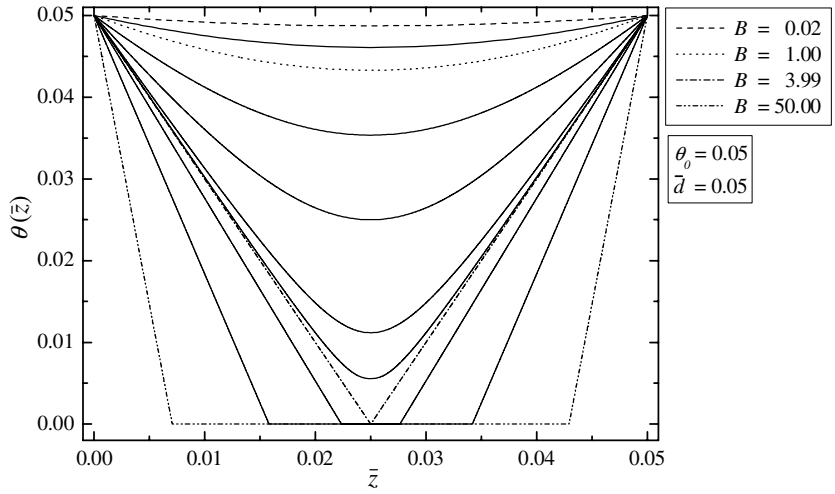

Figure 5. The solutions for $\theta(\bar{z})$ obtained from the implicit solutions given by equations (2.19) to (2.23) and (2.27) for the increasing B values 0.02, 0.6, 1, 2, 3.8, 3.95, 3.99, 5, 10 and 50 when the tilt angle of the director on the boundaries is set to $\theta_0 = 0.05$ radians and the sample depth $\bar{d} = 0.05$. The smooth extremal becomes a broken extremal as B increases. In this particular example broken extremals occur for $B > B^* \doteqdot 3.99$. The solutions for $B < B^*$, $B = B^*$ and $B > B^*$ correspond to the geometries depicted in figure 2(*a*), (*b*) and (*c*), respectively.

order below 10^{-2} for most surface pretilt angles θ_0, as can be seen from figure 3. This is one essential feature of the problem discussed in this section. The second key feature appears in figure 5: if the sample depth d is sufficiently large (so that $d > 2z_m^*$) then the sample enters the idealized SmA phase where $\theta \equiv 0$ for $z_m^* \leqslant z \leqslant d - z_m^*$, as shown in figure 2(*c*). Figure 5 shows such solutions for $\theta(\bar{z})$ where $\bar{z}_m^*$, which is the point closest to the boundary at $\bar{z} = 0$ where θ becomes zero, clearly decreases as B increases above B^*. The actual values of $\bar{d}$ and θ_0 used in the calculations of figure 5 are not particularly physically significant and have been chosen merely to allow the broken extremals and their properties, discussed above, to be more clearly visualized. For physically relevant values of $\bar{d}$ and θ_0 the boundary layers that arise in figure 5 will persist on a length scale of size $\bar{z}_m^*$ that will depend on B: the actual physical values for the penetration depth $\bar{z}_m^*$ can always be calculated via (2.23) and, from the above comments, B may be expected to be of the order 10^{-2} or smaller. Adopting physically relevant parameters will lead to graphs that look very similar to those in figure 5, the only difference being that many solutions would have $\theta \equiv 0$ across most of the sample with θ varying only in boundary layers very close to $\bar{z} = 0$ and $\bar{z} = \bar{d}$. These boundary layers would qualitatively be similar in appearance to those in figure 5, which shows the main qualities of the broken extremal solutions when they are available.

2.2. Bookshelf-aligned SmA

It is of interest to examine a similar set-up to the previous one, the main difference being that the smectic layers will now be generally perpendicular to the boundaries in a bookshelf type of alignment, as shown in figure 6. The approximate orientation of the smectic layers may be assumed planar and perpendicular to the boundary surfaces for some relatively small surface pretilt angle θ_0. Of course, the ideal problem should properly include some layer

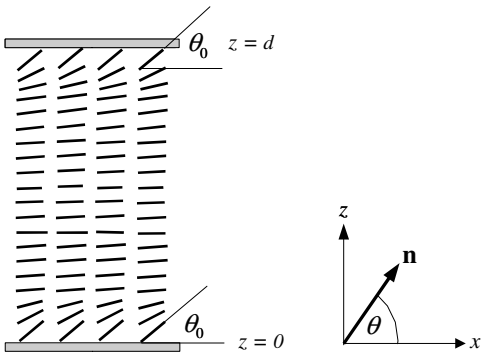

Figure 6. Exaggerated schematic view of a fixed 'bookshelf' SmA liquid crystal. The layers may be approximated as being fixed planar layers with some variation in the director orientation near the boundaries. The director is fixed on the boundaries at the pretilt angle θ_0, as shown.

reorientation near the boundaries, and this will be investigated in the following section for an experimentally relevant set-up that differs slightly from figure 6. It is the aim here to derive some analytic solutions for this simplified problem and thereby determine analytically an approximation to the behaviour of any boundary layer phenomena. Such results can only be obtained numerically for the full nonlinear problem to be discussed in the following section where θ_0 need not be small, as is known from experiments [5].

In the geometry of figure 6, $\Phi = x$ and the director and layer normal $\mathbf{a} = \nabla\Phi$ take the forms

$$\mathbf{n} = (\cos\theta(z), 0, \sin\theta(z)), \qquad \mathbf{a} = (1, 0, 0), \tag{2.31}$$

where the boundary conditions on $\theta(z)$ are again given by

$$\theta(0) = \theta(d) = \theta_0 > 0, \tag{2.32}$$

where θ_0 is the fixed pretilt angle of the director on the boundaries. In this case, the energy density (1.1) becomes

$$w = \tfrac{1}{2}K_1^n(\theta')^2\cos^2\theta + \tfrac{1}{2}B_0(1-\cos\theta)^2 + \tfrac{1}{2}B_1\sin^2\theta, \tag{2.33}$$

where a prime denotes $\mathrm{d}/\mathrm{d}z$ and, analogous to the previous situation at equations (2.3) to (2.6), the Euler–Lagrange equilibrium equation is

$$K_1^n\{\theta''\cos^2\theta - (\theta')^2\sin\theta\cos\theta\} - B_0\sin\theta(1-\cos\theta) - B_1\sin\theta\cos\theta = 0. \tag{2.34}$$

The symmetry and other requirements stated at equations (2.8) and (2.9) supplement the boundary conditions (2.32). Equation (2.34) can be integrated and non-dimensionalized by the same procedure as that carried out in equations (2.7) to (2.15) to find that the solution for θ as a function of the rescaled variable $\bar{z}$ is given implicitly by the analogue of the results stated in equations (2.15) and (2.16). Thus the solution is obtained via

$$\bar{z} = \int_{\theta}^{\theta_0} \frac{\cos\psi}{[(B-1)(\cos^2\theta_m - \cos^2\psi) + 2(\cos\theta_m - \cos\psi)]^{\frac{1}{2}}}\,\mathrm{d}\psi, \qquad 0 \leqslant \bar{z} < \frac{\bar{d}}{2}, \tag{2.35}$$

subject to the requirement, arising as before from (2.9)

$$\frac{\bar{d}}{2} = \int_{\theta_m}^{\theta_0} \frac{\cos\psi}{[(B-1)(\cos^2\theta_m - \cos^2\psi) + 2(\cos\theta_m - \cos\psi)]^{\frac{1}{2}}}\,\mathrm{d}\psi. \tag{2.36}$$

Similar to the previous solution, θ_m is determined from (2.36) for given values of $\bar{d}$, θ_0 and B; this value of θ_m is then inserted into (2.35) to complete the implicit solution for θ. Unlike the

previous solution requirement (2.16), the integral in (2.36) diverges as $\theta_m \to 0^+$ and hence θ_m must be strictly positive for any finite sample depth $\bar{d}$: there is no broken extremal available in this problem.

Solution (2.35) can be expressed in terms of elliptic integrals, the forms of which depend upon B. The substitution $u = \cos\psi$ transforms (2.35) and (2.36) to, respectively,

$$\bar{z} = \int_{\cos\theta_0}^{\cos\theta} G(B, \theta_m, u)\,\mathrm{d}u, \tag{2.37}$$

$$\frac{\bar{d}}{2} = \int_{\cos\theta_0}^{\cos\theta_m} G(B, \theta_m, u)\,\mathrm{d}u, \tag{2.38}$$

where

$$G(B, \theta_m, u) = u(1-u^2)^{-\frac{1}{2}}[(B-1)(\cos^2\theta_m - u^2) + 2(\cos\theta_m - u)]^{-\frac{1}{2}}. \tag{2.39}$$

The comments after (2.11) remain valid and therefore, since θ_0 and θ_m are non-zero, the denominator in (2.39) is always positive for $\cos\theta_0 \leqslant u < \cos\theta_m$. There are three cases to consider.

(i) $0 < B < 1$

In this case, we can write

$$G(B, \theta_m, u) = u\,[(1-B)(a_1-u)(a_2-u)(a_3-u)(u-a_4)]^{-\frac{1}{2}}, \tag{2.40}$$

where

$$a_1 = \frac{2}{1-B} - \cos\theta_m, \qquad a_2 = 1, \qquad a_3 = \cos\theta_m, \qquad a_4 = -1, \tag{2.41}$$

and it is further seen that

$$a_1 > a_2 > a_3 \geqslant \cos\theta > a_4. \tag{2.42}$$

Making use of (2.38), solution (2.37) is given by

$$\bar{z} = \int_{\cos\theta_0}^{\cos\theta} G(B, \theta_m, u)\,\mathrm{d}u = \frac{\bar{d}}{2} - \int_{\cos\theta}^{\cos\theta_m} G(B, \theta_m, u)\,\mathrm{d}u, \tag{2.43}$$

and it therefore has the representation ([15, section 3.148.3])

$$\bar{z} = \frac{\bar{d}}{2} - [(1 + (B-1)\cos\theta_m]^{-\frac{1}{2}}\{F(\gamma(\theta), k) + (\cos\theta_m - 1)\Pi(\gamma(\theta), n, k)\}, \tag{2.44}$$

where θ_m is obtained from (2.38) as a solution to the relation

$$\frac{\bar{d}}{2} = [1 + (B-1)\cos\theta_m]^{-\frac{1}{2}}\{F(\gamma(\theta_0), k) + (\cos\theta_m - 1)\Pi(\gamma(\theta_0), n, k)\}. \tag{2.45}$$

In these results, F and Π are the standard incomplete elliptic integrals of the first and third kinds ([15, section 8.111]), respectively, where $\gamma(\theta)$, n and the elliptic modulus k are defined by

$$\gamma(\theta) = \arcsin\sqrt{\frac{2(\cos\theta_m - \cos\theta)}{(1+\cos\theta_m)(1-\cos\theta)}}, \tag{2.46}$$

$$n = \frac{1}{2}(1 + \cos\theta_m), \tag{2.47}$$

$$k = \frac{1}{2}\sqrt{\frac{(1+\cos\theta_m)(B+1+(B-1)\cos\theta_m)}{(1+(B-1)\cos\theta_m)}}. \tag{2.48}$$

(ii) $B = 1$

In this case,

$$G(1, \theta_m, u) = \frac{u}{\sqrt{2}}[(a_2 - u)(a_3 - u)(u - a_4)]^{-\frac{1}{2}}, \tag{2.49}$$

where a_2, a_3 and a_4 are as defined above in (2.41) and similarly obey the inequalities in (2.42). The solution obtained from (2.37) and (2.38) can be written in the same style as (2.44) and (2.45) and is given by ([15, section 3.132.3])

$$\bar{z} = \frac{\bar{d}}{2} - \{F(\gamma(\theta), \sqrt{n}) + (\cos\theta_m - 1)\Pi(\gamma(\theta), n, \sqrt{n})\}, \tag{2.50}$$

where $\gamma(\theta)$ and n are as above and θ_m is obtained from the relation

$$\frac{\bar{d}}{2} = \{F(\gamma(\theta_0), \sqrt{n}) + (\cos\theta_m - 1)\Pi(\gamma(\theta_0), n, \sqrt{n})\}. \tag{2.51}$$

(iii) $B > 1$

For $B > 1$, we can write

$$G(B, \theta_m, u) = u[(B - 1)(u - a_1)(a_2 - u)(a_3 - u)(u - a_4)]^{-\frac{1}{2}}, \tag{2.52}$$

where a_1 to a_4 are as defined in (2.41), except that on this occasion, because $B > 1$, the inequalities in (2.42) should be replaced by

$$a_2 > a_3 \geqslant \cos\theta > \max\{a_1, a_4\} \geqslant \min\{a_1, a_4\}. \tag{2.53}$$

The solution obtained via (2.37) and (2.38), which is identical when the roles of a_1 and a_4 are interchanged, is given by ([15, section 3.148.5])

$$\bar{z} = \frac{\bar{d}}{2} - 2[(1 + \cos\theta_m)(B + 1 + (B - 1)\cos\theta_m)]^{-\frac{1}{2}}\{F(\chi(\theta), k^{-1}) + (\cos\theta_m - 1)\Pi(\chi(\theta), p, k^{-1})\}, \tag{2.54}$$

where the minimum angle θ_m is obtained from (2.38) as a solution of

$$\frac{\bar{d}}{2} = 2[(1 + \cos\theta_m)(B + 1 + (B - 1)\cos\theta_m)]^{-\frac{1}{2}}\{F(\chi(\theta_0), k^{-1}) + (\cos\theta_m - 1)\Pi(\chi(\theta_0), p, k^{-1})\}. \tag{2.55}$$

In these results k remains as defined by equation (2.48), while $\chi(\theta)$ and the parameter p are defined by

$$\chi(\theta) = \arcsin\sqrt{\frac{(B + 1 + (B - 1)\cos\theta_m)(\cos\theta_m - \cos\theta)}{2(1 + (B - 1)\cos\theta_m)(1 - \cos\theta)}}, \tag{2.56}$$

$$p = \frac{2(1 + (B - 1)\cos\theta_m)}{(B + 1 + (B - 1)\cos\theta_m)}. \tag{2.57}$$

Figure 7(*a*) shows the above solutions calculated for the case where $\theta_0 = 0.5$ radians and $\bar{d}$ has been fixed at 20. They are qualitative solutions which show the influence of the non-dimensionalized coupling constant B for fixed values of θ_0 and $\bar{d}$. Boundary layers appear as B increases. If $\theta(\bar{z})$ is close to zero, then the governing equilibrium equation (2.34) may be linearized in θ and its derivatives so that the problem and its boundary conditions may be approximated by

$$\theta'' - B\theta = 0, \qquad \text{with} \qquad \theta(0) = \theta(\bar{d}) = \theta_0, \qquad \theta'\left(\frac{\bar{d}}{2}\right) = 0, \tag{2.58}$$

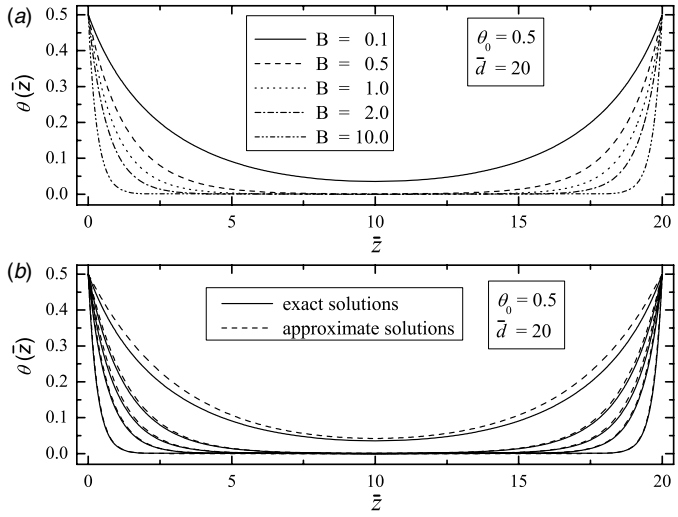

Figure 7. (*a*) Solutions to the 'rigid' smectic layer approximation, motivated by figure 6, obtained via equations (2.44), (2.50) and (2.54) for the indicated values of B. The director is fixed on the boundaries at $\theta_0 = 0.5$ radians and, for illustration, $\bar{d}$ has been set to 20. (*b*) A comparison between the solutions in (*a*) (solid lines) and the corresponding approximate solutions (dashed lines) given by equation (2.59) for the same values of θ_0 and $\bar{d}$. Boundary layers appear near $\bar{z} = 0$ and $\bar{z} = 20$ and occur on a length scale ξ where $\xi \approx 1/\sqrt{B}$, as discussed in the text.

where a prime now denotes $\mathrm{d}/\mathrm{d}\bar{z}$. The corresponding solution is

$$\theta(\bar{z}) = \theta_0 \,\mathrm{sech}(\sqrt{B}\bar{d}/2)\cosh(\sqrt{B}(\bar{d} - 2\bar{z})/2). \tag{2.59}$$

A comparison of this approximate solution with the exact solutions presented in figure 7(*a*) is made in figure 7(*b*), where the solid lines represent the solutions in figure 7(*a*) and the nearby dotted lines represent the corresponding approximate solutions obtained from (2.59) for the same values of B. There is good agreement between the exact and approximate solutions for $B > 1$. Solution (2.59) shows that there are boundary layers occurring over the (dimensionless) length scale ξ, where $\xi = 1/\sqrt{B}$. A similar effect in the context of variable smectic layers will be seen in the following section. It is clear from figure 7 that θ is close to zero across most of the sample in the bulk for large values of B, which indicates that most of the alignment will be bookshelf SmA except near the boundary layers. As mentioned previously, it is expected that λ will be roughly of the same size as the smectic interlayer distance d_0 (perhaps around 20 Å–50 Å) and so, by the definition of $\bar{z}$ in (2.14), a boundary layer with ξ below 5 (see figure 7) indicates that the director will more or less conform to the SmA structure within a small number of smectic layers from the boundary: this effect, which will also be notable in the nonlinear variable layer problem to be discussed in the following section, is perhaps typical of confined smectics.

3. Variable smectic layers

In this section, we consider the nonlinear problem of a bookshelf-type geometry where the director **n** and smectic layer normal **a** can decouple with **a** no longer constrained to be constant. The director and smectic layer alignments will be assumed uniform in the x and y directions so that the orientation angles θ and δ for **n** and **a**, respectively, are functions of z only, each

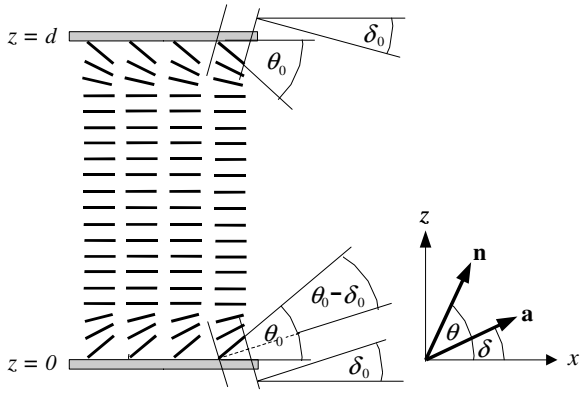

Figure 8. A schematic view of a bookshelf SmA liquid crystal which allows both the director and smectic layer structure to vary. The orientation angles for the director **n** and smectic layer normal **a** are θ and δ, respectively, measured relative to the x-axis. The usual smectic cone angle is defined as the difference between θ and δ.

measured relative to the x-axis as shown in figure 8. We shall consider a sample of smectic liquid crystal of unit cross-sectional area in the xy plane and depth d in the z direction arranged as in figure 8: this set-up has been motivated by the experimental work of Elston [5]. The usual smectic cone angle, which is always measured relative to the layer normal direction, is now defined by $|\theta(z) - \delta(z)|$. Strong anchoring of the director will be supposed and therefore we shall set θ to be the fixed angle θ_0 at the lower boundary $z = 0$ and, by symmetry, $-\theta_0$ at the upper boundary $z = d$. It will also be assumed that the smectic layers exhibit a fixed layer tilt δ_0 at $z = 0$ and $-\delta_0$ at $z = d$.

In the context of the present theory, the director **n** and the smectic layer representation Φ can take the forms

$$\mathbf{n} = (\cos\theta(z), 0, \sin\theta(z)), \tag{3.1}$$

$$\Phi(x, z) = x + \int_{z_0}^{z} \tan\delta(t)\,\mathrm{d}t, \tag{3.2}$$

where z_0 is an arbitrary constant. It is clear from (3.2) that, provided $0 \leqslant \delta < \frac{\pi}{2}$,

$$\nabla\Phi = (1, 0, \tan\delta(z)), \qquad |\nabla\Phi| = \sec\delta(z), \tag{3.3}$$

$$\mathbf{a} \equiv \frac{\nabla\Phi}{|\nabla\Phi|} = (\cos\delta(z), 0, \sin\delta(z))\,, \tag{3.4}$$

$$\mathbf{n}\cdot\mathbf{a} = \cos(\theta(z) - \delta(z)). \tag{3.5}$$

The expression for $\Phi(x, z)$ in (3.2) can be derived from quite general results on quasi-linear partial differential equations by considering the solution to (3.4) for Φ as a function of x and z [16]. Thus **n** and **a** are allowed to vary yet remain precisely unit vectors. A brief discussion about how the form for Φ introduced in equation (3.2) relates to the general expressions available in the literature is contained in appendix A.2. It should also be mentioned here that $\nabla\Phi$ above is similar in style to a variable magnitude vector in the direction of the smectic layer normal introduced, in a different mathematical model and context, by Anderson and Leslie [17], who did not consider the function Φ explicitly.

The above expressions can be inserted into the energy density (1.1) to find that

$$w = \tfrac{1}{2}K_1^n(\theta')^2\cos^2\theta + \tfrac{1}{2}K_1^a(\delta')^2\cos^2\delta + \tfrac{1}{2}B_0\,[\sec\delta + \cos(\theta-\delta) - 2]^2 + \tfrac{1}{2}B_1\sin^2(\theta-\delta), \tag{3.6}$$

where a prime denotes differentiation with respect to z. The equilibrium solutions must satisfy the coupled Euler–Lagrange equations ([14, p 92]) for (3.6). These equilibrium equations are

$$K_1^n[\theta''\cos^2\theta - (\theta')^2\sin\theta\cos\theta] + B_0[\sec\delta + \cos(\theta-\delta) - 2]\sin(\theta-\delta) - B_1\sin(\theta-\delta)\cos(\theta-\delta) = 0, \tag{3.7}$$

$$K_1^a[\delta''\cos^2\delta - (\delta')^2\sin\delta\cos\delta] - B_0[\sec\delta + \cos(\theta-\delta) - 2][\sec\delta\tan\delta + \sin(\theta-\delta)] + B_1\sin(\theta-\delta)\cos(\theta-\delta) = 0, \tag{3.8}$$

with the accompanying boundary conditions following from figure 8, namely,

$$\theta(0) = \theta_0, \qquad \theta(d) = -\theta_0, \qquad \delta(0) = \delta_0, \qquad \delta(d) = -\delta_0. \tag{3.9}$$

These equations can be non-dimensionalized via the variables introduced in equation (2.14). Doing so reveals that they can be written as

$$\theta''\cos^2\theta - (\theta')^2\sin\theta\cos\theta + [\sec\delta + \cos(\theta-\delta) - 2]\sin(\theta-\delta) - B\sin(\theta-\delta)\cos(\theta-\delta) = 0, \tag{3.10}$$

$$\kappa[\delta''\cos^2\delta - (\delta')^2\sin\delta\cos\delta] - [\sec\delta + \cos(\theta-\delta) - 2][\sec\delta\tan\delta + \sin(\theta-\delta)] + B\sin(\theta-\delta)\cos(\theta-\delta) = 0, \tag{3.11}$$

where a prime now denotes differentiation with respect to $\bar{z}$, $\kappa = K_1^a\big/K_1^n$ represents a measure for the anisotropy in the elastic constants and the boundary conditions are

$$\theta(0) = \theta_0, \qquad \theta(\bar{d}) = -\theta_0, \qquad \delta(0) = \delta_0, \qquad \delta(\bar{d}) = -\delta_0. \tag{3.12}$$

The main dimensionless control parameters for solutions to this problem are therefore κ and B. Motivated by figure 8, we shall seek solutions to equations (3.10) to (3.12) which obey the relations

$$\theta(\bar{z}) = -\theta(\bar{d} - \bar{z}), \qquad \delta(\bar{z}) = -\delta(\bar{d} - \bar{z}), \qquad \text{for} \qquad 0 \leqslant \bar{z} \leqslant \bar{d}, \tag{3.13}$$

and find solutions on the interval $0 \leqslant \bar{z} \leqslant \bar{d}/2$. The solutions for $\bar{d}/2 \leqslant \bar{z} \leqslant \bar{d}$ are obtained via the requirements in (3.13).

The nonlinear differential equations (3.10) and (3.11) subject to the boundary conditions (3.12) can be solved numerically for given values of B, κ, θ_0, δ_0 and $\bar{d}$ by means of the dsolve routine in Maple [18]. For illustrative purposes, we shall take fixed values of θ_0, δ_0 and $\bar{d}$, and display solutions for a selection of values for the parameters κ and B. Figure 9 shows typical solutions for θ and δ when $\bar{d} = 1000$, $\kappa = 1$, $B = 1$, $\theta_0 = \pi/6$ and $\delta_0 = \pi/18$: other parameter values give qualitatively similar plots. Two features are apparent: the first is that θ and δ virtually coincide except for small regions close to the boundaries and the second is that the sample is effectively in the bookshelf SmA structure not far from the boundaries, that is, θ and δ are very close to zero across the bulk of the sample. This means that there are essentially two boundary layer phenomena. The first boundary layer effect occurs as the director and layer normal reorient to become mutually parallel (where $\theta \simeq \delta$) within a short distance from the boundary, which indicates that the sample adopts the SmA phase not far from the boundary. The smectic layers are still tilted, in the sense that δ is non-zero, during this process. The second boundary layer effect occurs as the smectic layers themselves reorient as

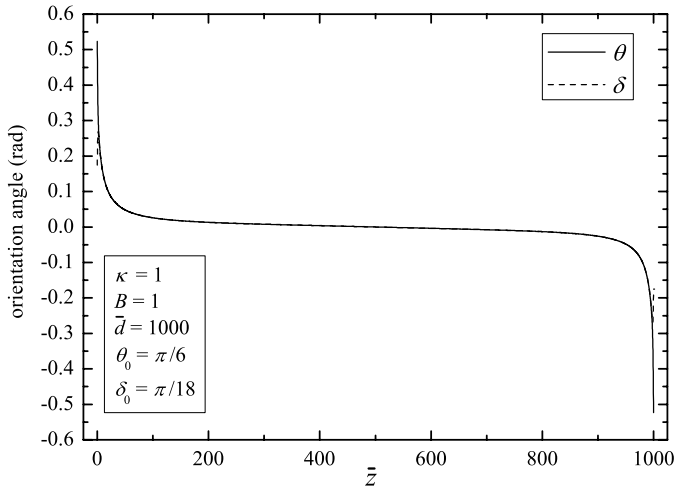

Figure 9. Solutions to equations (3.10) to (3.12) for the director orientation angle θ and layer tilt δ obtained numerically. The solutions for θ and δ almost coincide in the bulk of the sample, which is also very close to the SmA bookshelf alignment (where $\delta \approx 0$) over the centre of the sample. Boundary layer phenomena occur: see figure 10(a) for the solutions near $\bar{z} = 0$.

they attempt to adopt a preferred bookshelf structure. This process takes place over a distance from the boundary that is larger than that over which **n** and **a** reorient to coincide in the first boundary layer effect, but is relatively small compared to the overall sample depth $\bar{d}$. These effects are best displayed in figure 10, where $\theta_0 = \pi/6$, $\delta_0 = \pi/18$ and $\bar{d} = 1000$ in all plots. Figure 10(a) shows precisely the same solutions that are in figure 9 for θ and δ when $\kappa = 1$ and $B = 1$, except that the $\bar{z}$-axis has now been presented on a log scale for $0 < \bar{z} \leqslant \bar{d}/2$ in order to show the extent of the boundary layer phenomena. The remaining graphs in figure 10 show solutions for θ and δ for the same boundary conditions as κ and B vary. All these graphs confirm the presence of the same underlying structure that has been discussed above, namely, two boundary layer phenomena. The first boundary layer effect is evident as θ and δ gradually coincide. This happens over a distance ξ that can be approximated as $\xi = 1/\sqrt{B}$, as has been identified in section 2.2 for a problem with a fixed smectic layer approximation. There is an increase in ξ as B decreases, in all cases, irrespective of the value of the anisotropy in the elastic constants κ. From figure 10, since, as mentioned above in section 2.1, we may approximate λ by the smectic interlayer distance $d_0 \approx 20$ Å, ξ corresponds to around 50 Å–100 Å, obtained via the relation $z = \bar{z}\lambda$. This result compares favourably with the experimental data reported by, for example, Chen *et al* [19] for a ferroelectric smectic liquid crystal. The examples in figure 10 also show that the smectic layer structure is close to bookshelf-aligned SmA on a length scale of around 200 from the boundary, which corresponds to around 0.4 μm, with $\kappa = 10$ showing how a larger value for K_1^a relative to K_1^n extends the width of this boundary layer effect for the reorientation of the smectic layers. In summary, as $\bar{z}$ increases from zero the director and layer normal first manoeuvre to align parallel to each other and then the layer normal, which at this stage is more or less coincident with the director, begins to reorient parallel to the x-axis to form a bookshelf alignment. A similar situation arises as $\bar{z}$ decreases from $\bar{d}$. Other values of θ_0 and δ_0, including the case when $\delta_0 > \theta_0$, produce results that display the same characteristics shown in figure 10.

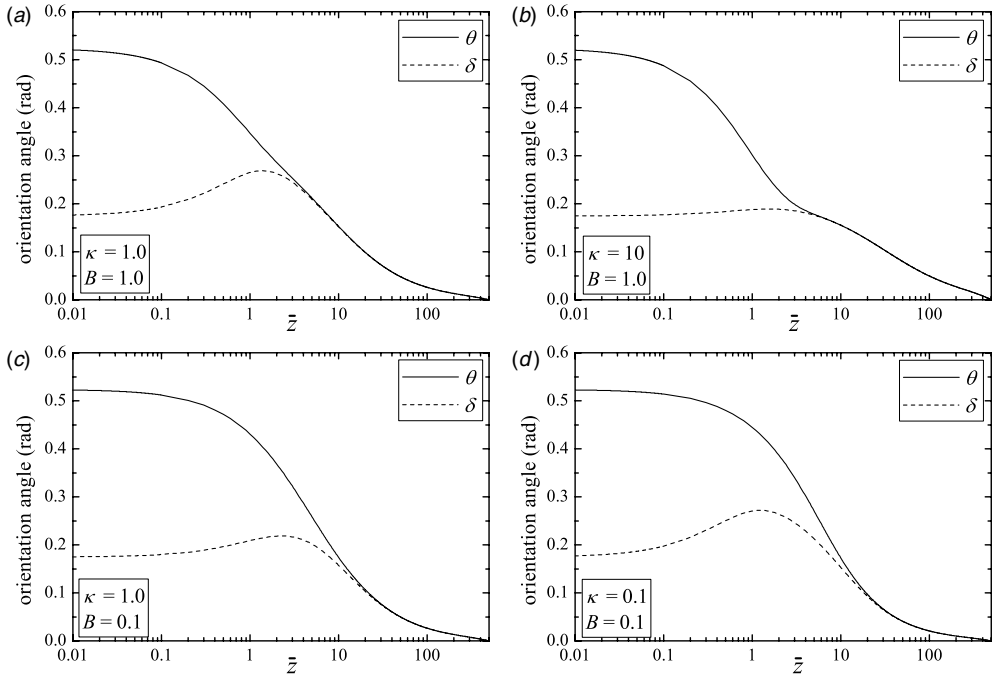

Figure 10. Solutions for θ (solid lines) and δ (dashed lines) for the indicated values of κ and B when the remaining parameters have been set as $\bar{d} = 1000, \theta_0 = \pi/6$ and $\delta_0 = \pi/18$. A log scale for $0 \leqslant \bar{z} \leqslant \bar{d}/2$ has been used to highlight the boundary layer effects. In all cases, θ and δ first become close over a relatively small distance from the boundary (roughly of order $1/\sqrt{B}$) compared to the layer structure, which is very close to the SmA bookshelf alignment ($\delta \approx 0$) at a distance of around 200 from the boundary. See the text for details. The plots in (*a*) are for the same solutions as in figure 9.

As mentioned earlier, Elston [5] employed the experimental set-up that has been investigated in this section and found that the smectic layer reorientation for samples of the liquid crystal SCE12 with a surface pretilt of $\theta_0 = \pi/6$ (as in figure 10) occurred over a region of about 0.5 μm near the boundaries. As observed from figure 10 and the comments above, the width of the region over which the smectic layers reorient to the bookshelf alignment is approximately 200: this therefore corresponds to a physical width of the same order of magnitude as that observed experimentally by Elston and also agrees with the results reported by Bonvent *et al* [20].

4. Discussion

This paper has examined three equilibrium configurations of SmA liquid crystals: a planar homeotropically aligned sample in section 2.1, a fixed smectic layer bookshelf approximation in section 2.2 and a particularly relevant experimental set-up in section 3 for a bookshelf alignment with a variable layer structure. A common feature throughout is the ability of the smectic energy density (1.1) to take into account the possibility of a decoupling of the director **n** from the smectic layer normal **a** so that they need not always necessarily coincide; **n** and **a** are often equated in other standard models. These examples also confirm that the penetration depth over which the director varies from being at a fixed pretilt angle θ_0 on the

boundaries to the SmA phase, where **n** is very close to **a**, is always of the order of a small multiple of the smectic interlayer distance d_0, as has been observed experimentally (e.g., [19]). As discussed above, typical estimates show this penetration depth to be around 50 Å–100 Å. The dimensionless penetration depth can be approximated in the bookshelf geometry by $\xi = 1/\sqrt{B}$, as identified in section 2.2. The range of values for B needed to achieve the analogous depth $\bar{z}_m^*$ for the homeotropically aligned planar geometry discussed in section 2.1 requires B to be considerably smaller than the values adopted in sections 2.2 and 3. This may indicate that the coupling between **n** and **a**, reflected in the value of B_1 appearing in equation (1.1), needs to be relatively weak in the homeotropically aligned planar geometry compared to that required for the bookshelf geometry: this interpretation demands further justification and investigation. Recall that in the introduction it was pointed out that the magnitude of B_1 should be comparable to that of B_0 or smaller [8].

The main results come from solutions to the coupled nonlinear differential equations that arise from the model in section 3 which allows both **n** and **a** to vary in a bookshelf-type-aligned sample with a strongly anchored director pretilt on the boundary surfaces. A nonlinear form for the smectic layer description function Φ was introduced in equation (3.2). When linearized, it can be identified with a function that is widely employed for small smectic layer displacements or distortions, as shown in appendix A.2. As mentioned in section 3, what appears to be two boundary layer effects take place over different length scales: the first occurs as **n** and **a** each reorient to coincide and the second occurs as the smectic layers adjust to adopt a bookshelf geometry. It was shown that **n** and **a** first attempt to mutually coincide to form an idealized SmA layer structure that remains tilted relative to the plane of the boundaries; this happens over a penetration depth of order $5d_0 \sim 10d_0$. However, beyond this initial penetration depth these SmA layers themselves reorient over a distance that is appreciably larger in order to achieve a preferred SmA bookshelf alignment in the central region of the sample: for typical parameter values it is of the order of $200d_0$, which corresponds to around 0.4 μm. Such results are evident in figure 10. Therefore, the distance from the boundary over which a sample, having the director at a fixed pretilt on the boundary, effectively becomes a bookshelf SmA is typically of this order. This is in qualitative agreement with the experimental observations of Elston [5]. A more detailed analysis of the boundary layer effects and their associated length scales may be possible by utilizing perturbation methods.

The equilibrium structures discussed in sections 2 and 3 for the planar and bookshelf geometries may vary upon the introduction of an externally applied electric or magnetic field or an applied dilative strain. The energy density (1.1) could be supplemented by the appropriate additional energy density. This often leads to a Helfrich–Hurault type of smectic layer instability that is well known when $\mathbf{n} \equiv \mathbf{a}$ and samples are subjected to applied fields [6, 7]. These, and other effects such as layer buckling [21], may also occur under dilative or compressive stresses [8]. Work is in progress to examine such phenomena in the context of the model introduced in this paper, especially in relation to the dynamics of distorted smectic layers based on the theory in [4]. Structures other than those considered here may also be investigated by the above methods, especially in relation to the alignments of SmA samples under high magnitude electric fields: progressive distortions of the smectic layers may lead to disclinations and focal conics, and a theoretical investigation may be feasible that will model the responses reported by Findon, Gleeson and Lydon [22]. The model in section 3 has not taken into account the possible occurrence of such defects or dislocations, especially near the boundaries.

The methods adopted in the paper can be applied to other energy density models for smectic liquid crystals, for example ferroelectric smectics. An energy density w that reflects the biaxiality induced as **n** and **a** decouple could be constructed for such smectic liquid crystals,

based upon those known for SmC and SmC* phases [6, 7, 23]. The chirality of these phases would require that ϕ, introduced in figure 1(*c*), varies as the director and layer structure distort since it could no longer be generally considered as fixed.

The Oseen constraint [24] for smectic liquid crystals, which has been used extensively in static theories [6, 7], states that $\nabla \times \mathbf{a} = \mathbf{0}$ in the absence of layer defects. This rather restrictive requirement has not been imposed here in order that some flexibility in the layer structure may appear as the director reorients, as is the case in section 3. Near the boundaries the Oseen constraint cannot be identically satisfied if the layers are allowed to distort relative to the director as it attempts to adopt the alignment of the idealized SmA phase; edge dislocations (cf ([25], p 302)) may occur and further analysis is required. Strong anchoring of the director and the layer orientation at the boundaries, a common assumption in the initial investigation of liquid crystal problems, has been supposed here, and it would be of interest to relax this condition to allow some weak anchoring at the boundaries. This could be achieved by adding a suitable surface energy to the energy W in (1.2) and seeking solutions to the corresponding coupled equilibrium equations arising from the bulk and surface energy contributions; this process will be analogous to that used for weakly anchored nematic liquid crystals under an applied magnetic field ([7], section 3.6).

Acknowledgments

The Author is indebted to the referees for their valuable comments, especially those related to the identification of a more general layer function Φ for the problem discussed in section 2.1. This has led to further developments that are currently in progress [16] and beyond the scope of this present paper.

Appendix A

A.1. As mentioned in section 1, the simplified energy density for planar-aligned SmA employed by Ribotta and Durand [8, equation (2)] for SmA under an applied strain can be derived from the nonlinear energy density (1.1). This is accomplished by letting ϕ be the angle between $\mathbf{n}$ and $\mathbf{a}$, so that $\mathbf{n} \cdot \mathbf{a} = \cos\phi \approx 1 - \phi^2/2$, and setting (cf [26])

$$K_1^a \equiv 0, \qquad \Phi = z - (Xz + u(x, z)), \tag{A.1}$$

where X is the strain and $u(x, z)$ is the smectic layer displacement function, which is assumed to be independent of y for the present discussion. When X and u vanish then $\Phi = z$, which represents planar-aligned smectic layers with the layer normal given by $\mathbf{a} = (0, 0, 1)$. For $|X| \ll 1$, to second order in u and ϕ (and their derivatives) we have

$$\nabla\Phi = (-u_x, 0, 1 - (X + u_z)), \qquad |\nabla\Phi| = 1 - X - u_z + \tfrac{1}{2}u_x^2, \tag{A.2}$$

and consequently $\mathbf{n}$ and $\mathbf{a} = \nabla\Phi/|\nabla\Phi|$ can be approximated by

$$\mathbf{n} = (-(\phi + u_x), 0, 1 - (\phi + u_x)^2/2), \qquad \mathbf{a} = \left(-u_x(1 + X + u_z), 0, 1 - u_x^2/2\right), \tag{A.3}$$

where the subscripts denote partial differentiation with respect to the indicated variables. These forms also follow naturally from geometrical considerations [8]. Note that $\mathbf{n}$ and $\mathbf{a}$ are unit vectors to second order. We can then confirm, to second order, that

$$\mathbf{n} \cdot \mathbf{a} = 1 - \tfrac{1}{2}\phi^2, \tag{A.4}$$

$$(\nabla \cdot \mathbf{n})^2 = (u_{xx} + \phi_x)^2. \tag{A.5}$$

Inserting $(A.1)_1$, $(A.2)_2$, (A.4) and (A.5) into equation (1.1) leads to the energy density that appears in [8] (with some obviously different notation for the constants K_1^n, B_0 and B_1), namely,

$$w = \tfrac{1}{2}K_1^n(u_{xx} + \phi_x)^2 + \tfrac{1}{2}B_0\left\{(X + u_z)^2 + X\phi^2 - Xu_x^2\right\} + \tfrac{1}{2}B_1\phi^2, \tag{A.6}$$

provided only terms to second order in u and ϕ are retained.

A.2. We briefly consider here the relationship between the general layer function introduced in equation (3.2) and that currently available in the literature when $\mathbf{n} \equiv \mathbf{a}$. In general, for a bookshelf-aligned geometry such as that shown in figure 8, it is common to write

$$\Phi(x, y, z) = x - u(x, y, z), \tag{A.7}$$

where $u(x, y, z)$ is the smectic layer displacement. For a more general discussion of this form in other geometries see [27]. When there is no variation to the planar bookshelf structure then $u \equiv 0$, $\Phi = x$ and $\mathbf{a} = (1, 0, 0)$. However, for a variable layer structure

$$|\nabla\Phi| = \left(1 - 2u_x + u_x^2 + u_y^2 + u_z^2\right)^{\frac{1}{2}} = 1 - u_x + \tfrac{1}{2}\left(u_y^2 + u_z^2\right) + \text{ higher order terms.} \tag{A.8}$$

Thus if higher order terms in the derivatives of u are neglected then the layer compression energy density, w_c say, is

$$w_c = \tfrac{1}{2}B_0(|\nabla\Phi| - 1)^2 \doteq \tfrac{1}{2}B_0\left(u_x - \tfrac{1}{2}\left(u_y^2 + u_z^2\right)\right)^2, \tag{A.9}$$

which, for the geometry introduced here, coincides with the well-know form for the smectic layer compression energy ([7, p 281]) when $\mathbf{a}$ and $\mathbf{n}$ are identical. If it is anticipated that u will depend only upon z for a particular reorientation of the layers, as is the case in this paper, then the compression energy density reduces to

$$w_c = \tfrac{1}{8}B_0u_z^4. \tag{A.10}$$

This expression can be recovered from the definition of Φ in equation (3.2) by setting

$$u = -\int_{z_0}^{z} \tan\delta(t)\,\mathrm{d}t, \tag{A.11}$$

whereby $u_z = -\tan\delta$. Then, by (3.3), $|\nabla\Phi| = \sec\delta = \left(1 + u_z^2\right)^{\frac{1}{2}} \doteq 1 + \tfrac{1}{2}u_z^2$ and so

$$w_c = \tfrac{1}{2}B_0(|\nabla\Phi| - 1)^2 \doteq \tfrac{1}{8}B_0u_z^4, \tag{A.12}$$

which agrees with (A.10). This expression for w_c is also equivalent to the corresponding contribution to the energy density in equation (3.6) if δ is set equal to θ and the resulting expression is taken to fourth order in δ.

References

[1] Auernhammer G K, Brand H R and Pleiner H 2000 *Rheol. Acta* **39** 215–22
[2] Auernhammer G K, Brand H R and Pleiner H 2002 *Phys. Rev.* E **66** 061707
[3] Soddemann T, Auernhammer G K, Guo H, Dünweg B and Kremer K 2004 *Eur. Phys. J.* E **13** 141–51
[4] Stewart I W 2007 *Contin. Mech. Thermodyn.* **18** 343–60
[5] Elston S J 1994 *Liq. Cryst.* **16** 151–7
[6] de Gennes P G and Prost J 1993 *The Physics of Liquid Crystals* 2nd edn (Oxford: Oxford University Press)
[7] Stewart I W 2004 *The Static and Dynamic Continuum Theory of Liquid Crystals* (London: Taylor and Francis)
[8] Ribotta R and Durand G 1977 *J. Phys.* **38** 179–204
[9] Auernhammer G K, Brand H R and Pleiner H 2005 *Phys. Rev.* E **71** 049901(E)
[10] E W 1997 *Arch. Ration. Mech. Anal.* **137** 159–75
[11] Santangelo C D and Kamien R D 2005 *Proc. R. Soc.* A **461** 2911–21
[12] McKay G and Leslie F M 1997 *Euro. J. Appl. Math.* **8** 273–80

[13] McKay G 2004 *J. Non-Newton. Fluid Mech.* **119** 115–22
[14] Sagan H 1992 *Introduction to the Calculus of Variations* (New York: Dover)
[15] Gradshteyn I S and Ryzhik I M 1980 *Table of Integrals, Series and Products* 4th edn (New York: Academic)
[16] Walker A J and Stewart I W , in preparation
[17] Anderson C and Leslie F M 1999 *Mol. Cryst. Liq. Cryst.* **330** 609–16
[18] Waterloo Maple Inc. 2002 *Maple 8*
[19] Chen W, Ouchi Y, Moses T and Shen Y R 1992 *Phys. Rev. Lett.* **68** 1547–50
[20] Bonvent J J, van Haaren J A M M, Cnossen G, Verhulst A G H and van der Sluis P 1995 *Liq. Cryst.* **18** 723–31
[21] Geer R E, Singer S J, Selinger J V, Ratna B R and Shashidhar R 1998 *Phys. Rev.* E **57** 3059–62
[22] Findon A, Gleeson H F and Lydon J 2000 *Phys. Rev.* E **62** 5137–42
[23] Carlsson T, Stewart I W and Leslie F M 1992 *J. Phys. A: Math. Gen.* **25** 2371–4
[24] Oseen C W 1933 *Trans. Faraday Soc.* **29** 883–99
[25] Kléman M and Lavrentovich O D 2003 *Soft Matter Physics: An Introduction* (New York: Springer)
[26] Singer S J 2000 *Phys. Rev.* E **62** 3736–46
[27] Kléman M and Parodi O 1975 *J. Phys.* **36** 671–81